

CrystEngComm

Accepted Manuscript



This is an *Accepted Manuscript*, which has been through the Royal Society of Chemistry peer review process and has been accepted for publication.

Accepted Manuscripts are published online shortly after acceptance, before technical editing, formatting and proof reading. Using this free service, authors can make their results available to the community, in citable form, before we publish the edited article. We will replace this *Accepted Manuscript* with the edited and formatted *Advance Article* as soon as it is available.

You can find more information about *Accepted Manuscripts* in the [Information for Authors](#).

Please note that technical editing may introduce minor changes to the text and/or graphics, which may alter content. The journal's standard [Terms & Conditions](#) and the [Ethical guidelines](#) still apply. In no event shall the Royal Society of Chemistry be held responsible for any errors or omissions in this *Accepted Manuscript* or any consequences arising from the use of any information it contains.



Journal Name

ARTICLE

Sequential Single-Crystal-to-Single-Crystal Transformations Promoted by Gradual Thermal Dehydration in a Porous Metavanadate Hybrid

Received 00th January 20xx,
Accepted 00th January 20xx

DOI: 10.1039/x0xx00000x

www.rsc.org/

Jagoba Martín-Caballero,^a Ana San José Wéry,^b Beñat Artetxe,^c Santiago Reinoso,^c Leire San Felices,^d José Luis Vilas^{*,a,e} and Juan M. Gutiérrez-Zorrilla^{*,a,c}

The porous hybrid metavanadate $[\{\text{Cu}(\text{cyclam})\}(\text{VO}_3)_2] \cdot 5\text{H}_2\text{O}$ (**1**) (cyclam = 1,4,8,11-tetraazacyclotetradecane) undergoes thermally triggered sequential single-crystal-to-single-crystal (SCSC) transformations upon gradual dehydration to produce three new porous crystalline phases, namely $[\{\text{Cu}(\text{cyclam})\}(\text{VO}_3)_2] \cdot 3\text{H}_2\text{O}$ (**2**), $[\{\text{Cu}(\text{cyclam})\}(\text{VO}_3)_2] \cdot 1.3\text{H}_2\text{O}$ (**3**) and $[\{\text{Cu}(\text{cyclam})\}(\text{VO}_3)_2]$ (**4**). Compound **1** consists in a three-dimensional structure formed by metavanadate chains linked by $\{\text{Cu}(\text{cyclam})\}$ moieties in a hybrid open framework with two different types of hexagonal channels where water molecules of hydration are hosted. The SCSC transformations cause a rearrangement of the metavanadate chains in such a way that they contract when going from **1** to **2** and stretch back when **2** transforms into **3**. The size of the channels is also modified as the hybrid dehydrates. The transition from **2** to **3** produces the cleavage of a Cu–O bond and consequent coordination of a $\{\text{Cu}(\text{cyclam})\}$ moiety to a different $\{\text{VO}_4\}$ unit, which drastically decreases the size of the channel in the process. In contrast, total dehydration of **3** enlarges the channel in the anhydrous phase **4** due to the migration of another Cu atom. The reversibility of such transformations has been monitored by a combination of thermogravimetric and powder X-ray diffraction analyses. While **1** and **3** are stable in open-air conditions, **2** transforms back into **1** upon being exposed to air for three weeks. The anhydrous phase **4** rapidly rehydrates into **3** in contact with ambient moisture. Furthermore, **3** can also be transformed into the parent hybrid **1** when soaked in water for seven days. Therefore, all crystal transitions described herein are fully reversible by applying the appropriate conditions.

Introduction

Solid state single-crystal-to-single-crystal (SCSC) transformations of coordination polymers have recently acquired remarkable interest as they constitute a promising research field within the materials science.¹ Such transformations usually involve the cleavage and formation of coordination bonds, and hence they often result in dramatic structural modifications with changes in properties like the colour, magnetism, luminescence or the ability to adsorb different molecules.² The occurrence of SCSC phase transitions is a powerful tool to characterize the structure of the functional materials that result from applying a given external stimulus (heat, light, pressure, etc.), which are usually not

accessible by conventional direct synthetic routes.³ They allow the exact monitoring of how the location of atoms and molecules change within the structure as a result of the external stimulus and hence, detailed structural information can be achieved for a better understanding of the transformation mechanisms and their relationship with the properties subject of interest.⁴ However, this type of structural studies require the preservation of single crystallinity during the phase transitions, which is inherently difficult.⁴ In the case of polyoxometalate (POM) compounds,⁵ these difficulties appear to be even harder to overcome considering the low number of reports on associated SCSC transformation phenomena that can be found in the literature. In particular, temperature-dependent transitions in POM-based compounds are limited to only a few examples to our knowledge.⁶ These reports consist in the low temperature polymorphs $[\text{Tm}_2(\text{H}_2\text{O})_{14}(\text{H}_6\text{CrMo}_6\text{O}_{24})][\text{H}_6\text{CrMo}_6\text{O}_{24}] \cdot 16\text{H}_2\text{O}$ and $\text{C}(\text{NH}_2)_3)_6[\text{Mo}_7\text{O}_{24}] \cdot \text{H}_2\text{O}$, as well as the monitoring of the dehydration in the $\text{H}_5\text{PV}_2\text{Mo}_{10}\text{O}_{40} \cdot 36\text{H}_2\text{O}$ acid and in the porous hybrid material $[\text{Co}_2(\text{ppca})(\text{H}_2\text{O})(\text{V}_4\text{O}_{12})_{0.5}]$ (ppca = 4-(pyridine-4-yl)pyridine-2-carboxylic acid).

Polyoxometalates are a family of anionic metal oxide clusters with an unmatched range of physicochemical properties.⁷ They constitute ideal building blocks for targeting new multifunctional materials due to their diverse magnetic,

^a BCMaterials, Parque Tecnológico de Bizkaia, Edificio 500, 48160 Derio, Spain.

^b Departamento de Desarrollo Sostenible, Universidad Católica de Ávila, c/Canteros s/n, 05005 Ávila, Spain.

^c Departamento de Química Inorgánica, Facultad de Ciencia y Tecnología, Universidad del País Vasco UPV/EHU, P.O. Box 644, 48080 Bilbao, Spain.

^d Servicios Generales de Investigación SGIker, Facultad de Ciencia y Tecnología, Universidad del País Vasco UPV/EHU, P.O. Box 644, 48080 Bilbao, Spain.

^e Departamento de Química Física, Facultad de Ciencia y Tecnología, Universidad del País Vasco UPV/EHU, P.O. Box 644, 48080 Bilbao, Spain.

† Electronic Supplementary Information (ESI) available: FT-IR spectra, PXRD and TPRD patterns, TGA/DTA curves, structural figures and tables, and X-ray crystallographic data of **1**, **2**, **3** and **4** in CIF format. See DOI: 10.1039/x0xx00000x.

redox and catalytic properties.⁸ In combination with transition metal–organic complexes, POMs are able to behave as multidentate ligands in such a way that they often result interconnected by several metal–organic moieties to form porous frameworks with potential applications in gas storage, ion exchange, or catalysis.⁹ As of today, the preparation of such type of hybrids is one of the main research focuses in the current synthetic POM chemistry because it might allow the development of sophisticated molecule–based materials and devices.¹⁰

In the course of our investigations on polyoxometalate/metal–organic systems, we recently reported the fully reversible desorption/readsorption of water via SCSC transformations in four hybrid compounds containing [α -XW₁₂O₄₀]⁴⁻ Keggin–type anions (X= Ge or Si) and Cu^{II} complexes of tetradentate bis(aminopyridyl)–type ligands upon heating and air–exposure.¹¹ We are now expanding this type of crystallochemical studies to other POM families like polyoxovanadates, which have shown exceptional properties in catalysis and biomedicine,¹² and related N–donor ligands to determine whether this phenomenon is common to other classes of POM–based hybrids or represents just a serendipitous observation. We selected for our purpose the commercial macrocyclic polyamine 1,4,8,11–tetraazacyclotetradecane (cyclam) because of the strong affinity shown by this type of macrocyclic tetradentate polyamines toward certain metals,¹³ which has led to their use as models for molecular carriers in biological systems,¹⁴ as catalysts with active sites that mimic metalloenzymes,¹⁵ or as anti–HIV agents.¹⁶

Herein, we report the synthesis and crystallochemical characterization of a new porous hybrid compound built of metavanadate anions and {Cu(cyclam)} cationic complexes, namely [{Cu(cyclam)}(VO₃)₂].5H₂O (**1**). This compound undergoes three sequential and reversible SCSC transformations promoted by gradual dehydration upon heating. The dynamic structural modifications induced by the removal of the water molecules produce three new crystalline phases, namely [{Cu(cyclam)}(VO₃)₂].3H₂O (**2**), [{Cu(cyclam)}(VO₃)₂].1.3H₂O (**3**) and [{Cu(cyclam)}(VO₃)₂] (**4**). All of these new phases retain porosity and show channels with different sizes that are determined by the thermally–triggered structural modifications.

Experimental

Materials and Methods

The *tert*–butylammonium metavanadate precursor [(CH₃)₃CNH₃][VO₃] was synthesized according to literature methods and identified by infrared (FT–IR) spectroscopy.^{5a} All other chemicals were obtained from commercial sources and used without further purification. Carbon, hydrogen and nitrogen contents were determined on a Perkin–Elmer 2400 CHN analyzer. FT–IR spectra were obtained as KBr pellets on a SHIMADZU FTIR–8400S spectrometer (Fig. S1 and S2 in the Supplementary Information). Powder X–ray diffraction (PXRD)

patterns were collected from 3 to 121 °C every 2 °C and from 30 to 600 °C every 20 °C using a Bruker D8 Advance diffractometer and 2 θ steps of 0.033° in the 5 ≤ 2 θ ≤ 35° range (Fig. S3 and S4 in the Supplementary Information). Thermogravimetric and differential thermal analyses (TGA/DTA) were carried out from room temperature to 800 °C at a rate of 5 °C min⁻¹ on a TA Instruments 2960 SDT thermobalance under a 150 cm³ min⁻¹ flow of synthetic air (Fig. S5 and S6 in the Supplementary Information).

Synthetic Procedure

[[Cu(cyclam)](VO₃)₂].5H₂O (1**).** [(CH₃)₃CNH₃][VO₃] (0.100 g, 0.60 mmol) was dissolved in distilled water (20 mL) and the pH was adjusted to 9 with aqueous 1M NaOH. Then, a solution of CuSO₄.5H₂O (0.075 g, 0.30 mmol) and cyclam (0.040 g, 0.20 mmol) in distilled water (15 mL) was added dropwise. The mixture was refluxed for 2 h, cooled down to room temperature and the formed dark pink precipitate was filtered. The resulting dark purple solution was left to slowly evaporate at room temperature and purple block–like crystals suitable for X–ray diffraction were obtained after 3 days. Yield: 49 mg (30% based on V). Elemental analysis: Found: C, 9.29; H, 2.38; N, 3.96. Calc. for C₁₀H₃₄CuN₄O₁₁V₂: C, 9.74; H, 2.48; N, 4.26%. IR: ν_{max} /cm⁻¹ 3229s, 3165s, 2936m, 2878m, 1638m, 1474w, 1454w, 1442w, 1429w, 1389w, 1358w, 1312w, 1292w, 1253w, 1236w, 1105m, 1091w, 1074w, 1062w, 1016m, 1008m, 962vs, 920vs, 895m, 883s, 854s, 758s, 544w, 521w, 499m, 440m.

[[Cu(cyclam)](VO₃)₂].3H₂O (2**).** Single crystals of **1** were heated at 40 °C in an oven for one hour, which produced a colour change from dark purple to light purple.

[[Cu(cyclam)](VO₃)₂].1.3H₂O (3**).** Single crystals of **1** were heated in an oven at 60 °C for one hour, with their colour changing to dark pink.

[[Cu(cyclam)](VO₃)₂] (4**).** Single crystals of **1** were heated in an oven at 120 °C for one hour and a slight colour change to darker purple was observed.

X–ray Crystallography

Crystallographic data for compounds **1–4** are given in Table 1. Intensity data were collected on an Agilent Technologies SuperNova diffractometer, which was equipped with monochromated Mo K α radiation (λ = 0.71073 Å) and Eos CCD detector. The data collection temperature was 100 K for **1**. For **2** and **3**, the crystals were respectively heated to 313 and 333 K at a rate of 1 K min⁻¹ and subsequently cooled to 100 K to perform the full data collection. In the case of **4**, the crystals were heated to 393 K but cracked upon lowering the temperature to 100 K. Therefore, we had to perform the full data collection at high temperature instead.

Table 1 Crystallographic data for 1–4.

	1	2	3	4
empirical formula	C ₁₀ H ₃₄ CuN ₄ O ₁₁ V ₂	C ₁₀ H ₃₀ CuN ₄ O ₉ V ₂	C ₁₀ H _{26.7} N ₄ CuO _{7.3} V ₂	C ₁₀ H ₂₄ CuN ₄ O ₆ V ₂
fw (g mol ⁻¹)	551.83	515.80	485.77	461.75
Z	12	3	3	3
Z'	6	1.5	1.5	1.5
crystal system	triclinic	triclinic	triclinic	triclinic
space group	<i>P</i> -1	<i>P</i> -1	<i>P</i> -1	<i>P</i> -1
temperature (K)	100(2)	100(2)	100(2)	393(2)
<i>a</i> (Å)	16.4455(3)	8.0199(2)	8.6253(10)	8.751(2)
<i>b</i> (Å)	15.0098(5)	13.9524(6)	12.890(2)	13.094(3)
<i>c</i> (Å)	27.8995(7)	14.2588(5)	13.368(2)	13.364(3)
α (°)	79.513(2)	102.032(3)	103.208(14)	102.449(18)
β (°)	98.024(2)	101.742(3)	106.557(12)	101.653(19)
γ (°)	105.156(2)	97.560(3)	95.595(11)	101.148(19)
<i>V</i> (Å ³)	6505.5(3)	1502.39(10)	1365.7(4)	1418.7(6)
ρ_{calc} (g cm ⁻³)	1.690	1.710	1.772	1.621
μ (mm ⁻¹)	1.873	2.014	2.203	2.111
collected reflections	46122	9271	8867	8399
unique reflections (<i>R</i> _{int})	22908 (0.036)	5290 (0.017)	4794 (0.067)	4991 (0.097)
observed reflections [<i>I</i> > 2 σ (<i>I</i>)]	17910	4751	3280	2115
parameters	1558	406	334	316
<i>R</i> (<i>F</i>) ^a [<i>I</i> > 2 σ (<i>I</i>)]	0.046	0.029	0.089	0.108
<i>wR</i> (<i>F</i> ²) ^b [all data]	0.111	0.074	0.183	0.251
GoF	1.038	1.051	1.132	1.052

$$^a R(F) = \frac{\sum ||F_o - F_c| |}{\sum |F_o|}; \quad ^b wR(F_2) = \left[\frac{\sum [w(F_o^2 - F_c^2)^2]}{\sum [w(F_o^2)]} \right]^{1/2}$$

Data frames were processed (unit cell determination, analytical absorption correction with face indexing, intensity data integration and correction for Lorentz and polarization effects) using the CrysAlis software package.¹⁷ The structures were solved using OLEX2¹⁸ and refined by full-matrix least-squares with SHELXL-2014/6.¹⁹ Final geometrical calculations were carried out with Mercury²⁰ and PLATON²¹ as integrated in WinGX.²² Thermal vibrations were treated anisotropically for all non-H atoms. Hydrogen atoms of the organic ligands were placed in calculated positions and refined using a riding model with standard SHELXL parameters. The space within the channels occupied by the water molecules of hydration was calculated using HOLLOW²³ and visualized in PyMol.²⁴ CCDC 1404576 (1), 1404577 (2), 1404578 (3) and 1404579 (4) contain the supplementary crystallographic data for this paper. These data can be obtained free of charge from The Cambridge Crystallographic Data Centre via www.ccdc.cam.uk/data_request/cif.

Results and Discussion

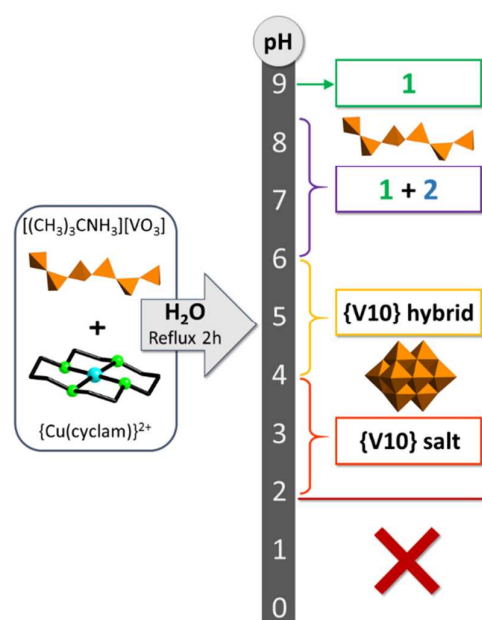
Synthesis

The synthesis of **1** was carried out by reacting *tert*-butylammonium metavanadate with cyclam and a copper(II) sulfate salt in aqueous medium at pH = 9. Different vanadate sources such as commercial Na(VO₃) and NH₄(VO₃), as well as the preformed [(CH₃)₃CNH₃](VO₃), were used to determine whether the counterions play any role in the formation of **1**.

Analogously, different copper(II) salts were also tested as the transition metal source (chloride, acetate and nitrate salts). No template effect of the cations was observed and all three metavanadate reagents led to compound **1**, although differences were observed in terms of yield and crystallization speed. The choice of the transition metal salt did neither affect the reaction in any apparent way. In contrast, the pH of the reaction medium has a key influence in the isolation of **1** as a pure crystalline phase (Scheme 1). When the pH was adjusted to basic values lower than 8.5, mixtures of **1** with crystals of a second metavanadate-containing hybrid phase (named as **2**) were obtained. Compound **1** was the major component in all of these mixtures as indicated by the PXRD patterns. Moreover, when the pH was lowered to values below 6, crystals of a decavanadate-containing hybrid species were isolated instead of **1** according to FT-IR spectroscopy. These crystals were obtained in trace amounts in mixtures with a yet unidentified powder. The full characterization of this decavanadate-containing hybrid is in progress and will be reported elsewhere. At pH values ranging from 4 to 2, a purely inorganic decavanadate salt was formed as indicated by the absence of any signal associated with organic molecules in the FT-IR spectra, whereas no identifiable solid product was obtained at pH values below 2.

Different reaction temperatures were also investigated (room temperature, 80 °C and reflux conditions). Compound **1** was obtained in all temperatures tested but we found that the reaction involving [(CH₃)₃CNH₃](VO₃) under reflux conditions (pH = 9) afforded the best yields. Moreover, differences in the

crystallization speed were also observed: the reactions at room temperature and 80 °C yielded crystals after approximately two weeks whereas **1** crystallized in just three days from that performed under refluxing conditions. Therefore, this particular synthetic system, while strongly dependent on the pH of the reaction media, it also appears to be affected by the temperature in a significant way. Although no synthetic conditions led to crystallization of compound **2** as a single crystalline phase, we found that pure batches of this compound could be prepared just by heating crystals of **1** at 40 °C for an hour, as it will be commented below. Analogously, compounds **3** and **4** could only be obtained by heating at 60 °C and 120 °C, respectively, samples of **1** or **2**, as we could not find any synthetic route to isolate them from solution. This fact nicely illustrates how thermally triggered solid–state reactions can provide access to compounds otherwise impossible to be prepared directly from solution reactions.



Scheme 1 Influence of the pH in the $\text{Cu}^{2+}:\text{cyclam}:\text{VO}_3^-$ synthetic system.

Thermo–structural behaviour

The thermal stability of compound **1** was investigated by TGA/DTA experiments. The thermal decomposition of **1** takes place in three mass loss stages (Fig. S5 in the Supplementary Information). The first stage is observed as an endothermic mass loss that extends from room temperature to temperatures around 120 °C and originates from the release of all water molecules of hydration. The mass loss (15.88%) corresponds to 5 water molecules per two vanadium atoms (calc. 16.30%). Dehydration leads to an anhydrous phase (**4**) that shows a significant range of thermal stability extending up to ca. 200 °C. Above this temperature, the anhydrous phase undergoes further decomposition via two overlapping mass loss stages of exothermic nature associated with the combustion of the organic ligands. The overall mass loss for this second stage (37.50%) is in good agreement with one

cyclam ligand per two vanadium atoms (calc. 37.17%). The final residue (46.6%) is obtained at temperatures above ca. 440 °C (calc for CuV_2O_6 : 47.4%).

Variable–temperature powder X–ray diffraction measurements (TPXRD) between 3 and 450 °C show that, as the dehydration proceeds, **1** transforms into two other crystalline phases before leading to the final anhydrous derivative (**4**), and hence two different partially hydrated intermediates must exist (Fig. S3 in the Supplementary Information). The temperatures at which these two solid–state phase transitions take place are 27 and 49 °C as shown in Fig. 1. The diffraction maxima within this range of temperatures corresponds to those observed for the minor component in the mixtures of crystalline phases obtained when the synthesis of **1** was carried out at basic values other than 9. Therefore, the first partially dehydrated intermediate observed in the TPXRD studies is the same compound **2** that co–crystallized with **1** in our systematic investigations on the influence of the pH in the $\text{Cu}^{2+}:\text{cyclam}:\text{VO}_3^-$ synthetic system. The transformation of the second partially hydrated intermediate (compound **3**) into the final anhydrous phase **4** is not as well defined as the two transitions mentioned above. The TPXRD patterns are not substantially modified from 49 to 120 °C (at which all water molecules of hydration are released according to the TGA curve), and only subtle variations can be observed in some of the diffraction maxima of weak intensity that appear at 2θ angles above 10°. For example, the two groups of signals in the $10 < 2\theta < 15^\circ$ range undergo a gradual change in their relative intensities that can be traced back to ca. 73 °C (Fig. S7 in the Supplementary Information), and this fact suggests that the final form of the hybrid $\{\text{Cu}(\text{cyclam})\}/\text{VO}_3$ framework in the anhydrous phase **4** is adopted above the latter temperature. This form is able to retain crystallinity upon total dehydration up to temperatures around 190 °C, in such a way that the anhydrous derivative **4** only becomes amorphous within the temperature range corresponding to the combustion of the organic ligands. The above results are in good agreement with the observations in the TGA curves of compound **1**. A new crystalline phase corresponding to the final residue starts appearing above 290 °C and reaches full formation at 450 °C. As shown in Fig. S8 in the Supplementary Information, this final residue has been identified as a mixture of the orthorhombic $Pmn2_1$ phase of V_2O_5 (PDF: 01-076-1803)²⁵ and the monoclinic $C2/c$ phase of $\text{Cu}_2\text{V}_2\text{O}_7$ (PDF: 01-073-1032)²⁶ in similar amounts. Traces of the orthorhombic $Pmn2_1$ phase of CuV_2O_6 (PDF: 00-016-0127)²⁷ have been detected as well.

It is well known that guest solvent molecules located in cavities or channels can often be removed from the open framework host material without causing its collapse, and furthermore, that they can also be reinserted sometimes. In order to explore this possibility, we decided to carry out single–crystal XRD studies in an attempt to determine the structure of the new crystalline phases that are formed during the dehydration process of **1**: the two partially dehydrated intermediates observed in the 27–49 and 49–73 °C ranges (**2** and **3**) and the anhydrous phase (**4**). A single crystal of **1** for

which full intensity data were initially collected at 100 K was selected, and the temperature was raised from room temperature to 40 °C at a rate of 1 °C min⁻¹. At this point, the temperature was lowered back to 100 K to perform a full data collection. The crystal preserved its integrity and crystallinity during the whole process and this allowed us to determine the structure of **2**. This process was repeated with a second crystal but the temperature was raised to 60 °C instead, which allowed us to structurally characterize the phase **3**. As mentioned above, the diffraction patterns do not undergo major changes from 49 to 190 °C (Fig. 1) and this suggests that the final anhydrous phase **4** shares a similar packing with the partially dehydrated intermediate **3**. To verify this observation, we attempted to perform the data collection of **4** by following an analogous procedure but heating at 120 °C. Unfortunately, the crystal cracked systematically when cooling down to 100 K, leading to datasets of poor quality. Therefore, we decided to skip the cooling stage and carried out the full data collection at 393 K. The diffraction data obtained at this temperature were of sufficient quality to refine the structure of **4** to acceptable final agreement factors.

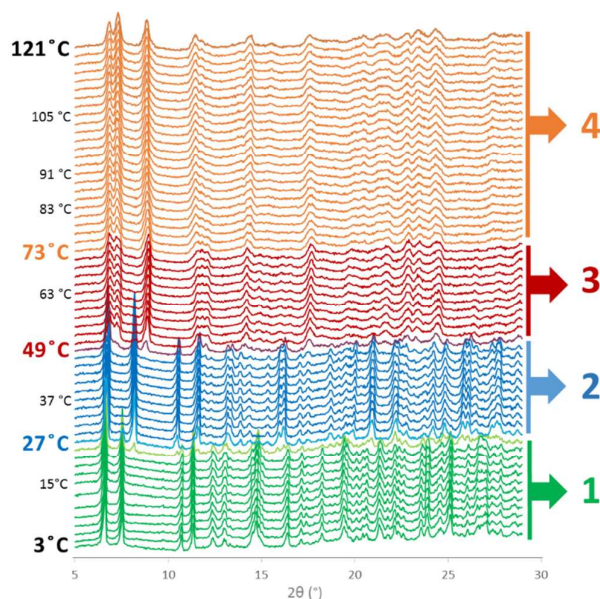


Fig. 1 Variable-temperature powder X-ray diffraction studies for **1**. The range of thermal stability for each crystalline phase and the temperatures at which the transformations take place are highlighted.

Crystal structure of **1**

Compound **1** crystallizes in the triclinic *P*-1 space group. The asymmetric unit of **1** contains two different vanadate fragments. Each fragment corresponds to a crystallographically independent metavanadate polymeric anion (Chain A and Chain B) and is built of six corner-sharing {VO₄} tetrahedra. The asymmetric unit is completed with six {Cu(cyclam)} complexes and thirty water molecules of hydration.

All of the six crystallographically independent {Cu(cyclam)} complexes found in **1** act as bridging metal-organic blocks between metavanadate chains. The coordination spheres of all

Cu^{II} centres show distorted octahedral geometries with the four N atoms of the cyclam ligand forming the equatorial plane and the axial positions occupied by terminal O atoms from different vanadate tetrahedra (Fig. 2). While all CuN₄O₂ chromophores show significant Jahn-Teller elongation, it must be noted that this type of distortion is especially remarkable for Cu1B and Cu1C as one of their respective axial Cu-O bonds show lengths near those of semi-coordination (Table S1 in the Supplementary Information). According to the literature, metal complexes of the cyclam ligand can adopt up to 5 different geometrical isomers depending on the ligand conformation, and more specifically, on whether the N-H bonds are located above or below the MN₄ plane²⁸ (Fig. S9 in Supplementary Information). All of the complexes found in the structure of **1** display a distorted-octahedral coordination environment with the so-called *trans-III* configuration, that is, two N-H bonds above and the other two below the CuN₄ equatorial plane. This is in perfect agreement with previous reports in the literature, which have shown that the most favourable configuration of a {Cu(cyclam)} complex with octahedral geometry is indeed the *trans-III* one.²⁹

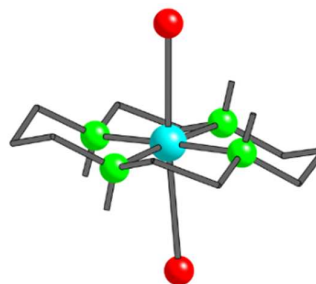


Fig. 2 Structure of the {Cu(cyclam)} complexes in **1-4** showing the *trans-III* configuration. Hydrogen atoms are omitted except those connected to N atoms. Colour code: Cu (blue), N (green), O (red).

The crystal packing of **1** can be described as a three-dimensional porous structure formed by metavanadate chains that extend along the *x* axis and are linked to neighbouring antiparallel chains by {Cu(cyclam)} bridging moieties in such a way that all {VO₄} tetrahedra display one complex anchored to a terminal O atom. This arrangement of polymeric anions and metal-organic complexes results in a hybrid open framework with two different types of hexagonal channels parallel to the [100] direction where all the water molecules are located (Fig. 3 and Fig. S10 in the Supplementary Information). The metavanadate chain A is formed by the six corner-sharing {VO₄} tetrahedra V1 to V6, whereas chain B consists of another six crystallographically independent VO₄ units labelled as V7 to V12. As shown in Fig. 4, the metal-organic complexes Cu1B, Cu1C, Cu1E and Cu1F link tetrahedra belonging to different chain types along the *y* axis, whereas Cu1A and Cu1D connect equivalent chains (type A and B, respectively) forming pairs along the *z* axis. Each pair of A-type chains is connected to four neighbouring pairs of B-type chains (and vice versa) in such a way that water containing hexagonal channels are generated. This connectivity originates two distinct type of channels, channel 1 (Ch1) and 2 (Ch2).

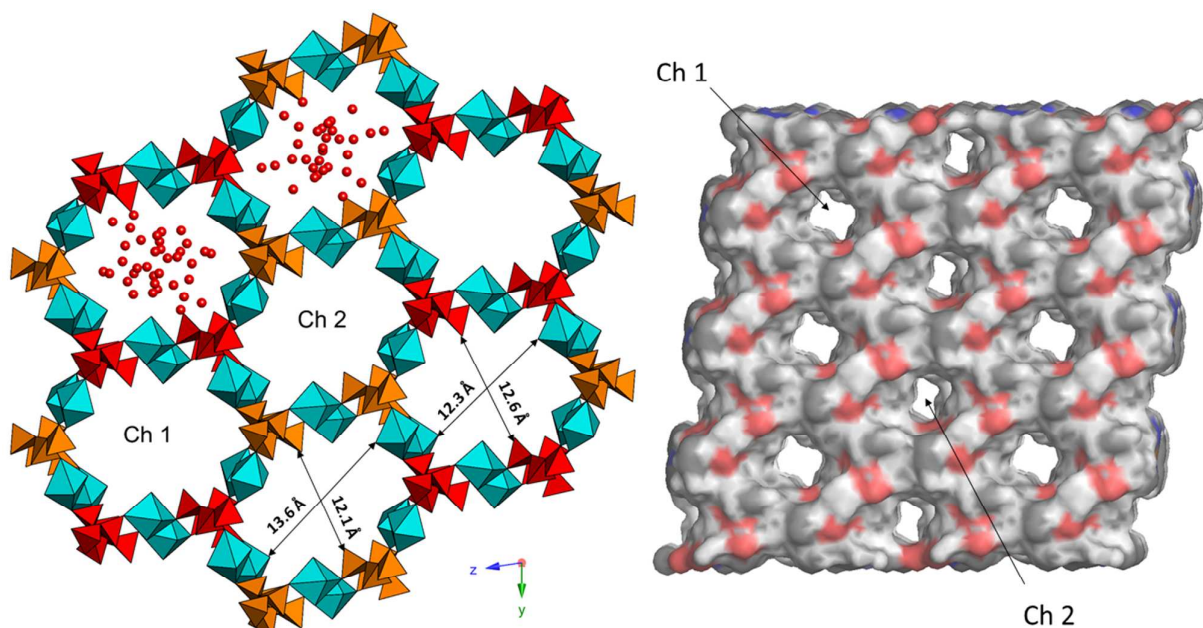


Fig. 3 Left: Crystal packing of **1** viewed along the x axis, showing the two different types of channels (Ch1 and Ch2) and details of the hosted water molecules and their estimated dimensions (the cyclam ligands are omitted for clarity; colour code: {VO₄} (orange: chain A; dark red: chain B), Cu (blue)). Right: Surface of the hybrid framework showing the different channels.

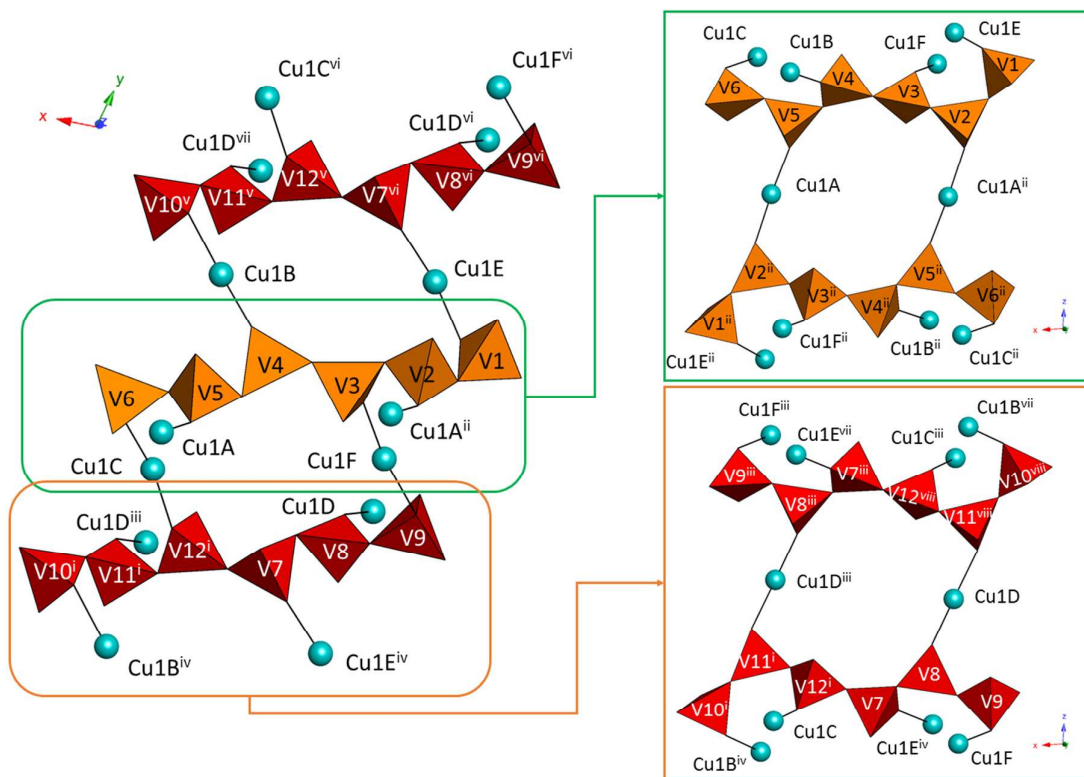


Fig. 4 Connectivity between metavanadate chains in compound **1** with atom labeling. The cyclam ligands and the water molecules are omitted for clarity. Colour code: {VO₄} (orange: chain A; dark red: chain B), Cu (blue). Symmetry codes: i) 1+x, y, z; ii) 1-x, 1-y, -z; iii) 1-x, -y, 1-z; iv) x, -1+y, z; v) 1+x, 1+y, z; vi) x, 1+y, z; vii) 1-x, 1-y, 1-z; viii) -x, -y, 1-z.

Each channel is delimited by four chains of one type and two chains of the second type (four A-type and two B-type for Ch1 and vice versa), which are connected by copper atoms with approximate cross sections of $12.6 \times 13.6 \text{ \AA}^2$ for Ch1 (distances O11M...O11M and N8C...N8C) and $12.1 \times 12.6 \text{ \AA}^2$ for Ch2 (distances O2M...O2M and N1F...N1F). The total solvent accessible volume is 1730 \AA^3 which corresponds to a 26% of the unit cell volume of **1**, as calculated using the PLATON software (Ch1: 922 \AA^3 , 14% and Ch2: 808 \AA^3 , 12%). An intricate network of C-H...O and N-H...O interactions between the cyclam ligands and the oxygen atoms of the metavanadate chains and some of the water molecules further contribute to the structural stability. Distances and angles of such interactions are compiled in Table S2 in the Supplementary Information.

The crystal packing of **1** is reminiscent of that found by Ou and coworkers in $[\{\text{CuL}\}(\text{VO}_3)_2] \cdot 0.33\text{H}_2\text{O}$,^{9e} where L stands for 5,5,7,12,12,14-hexamethyl-1,4,8,11-tetraazacyclotetradecane. However, some noticeable differences can be found between the structures of both compounds. While **1** shows two distinct types of distorted-hexagonal channels, $[\{\text{CuL}\}(\text{VO}_3)_2] \cdot 0.33\text{H}_2\text{O}$ displays only a single type of hexagonal channel with regular shape. This channel is significantly smaller than those found in **1** (754 \AA^3 , 14%) due to the strong steric hindrance effects induced by the methyl groups. Moreover, the channels in Ou's metavanadate hybrid constitute highly hydrophobic regions because the methyl groups point to the centre of the pores. This fact results in a significantly lower number of water molecules hosted within compared to those found in the hydrophilic pores of compound **1**.

Crystal structures of 2–4

Compounds **2–4** also crystallize in the triclinic *P*-1 space group, but in contrast to **1**, the asymmetric units of these compounds contain a single metavanadate chain fragment composed of only three corner-sharing $\{\text{VO}_4\}$ tetrahedra, together with three halves of $\{\text{Cu}(\text{cyclam})\}$ complexes located in inversion centres and coordinated to the vanadate polyhedra. Four and a half and two water molecules of hydration complete the asymmetric units of **2** and **3**, respectively. As observed for **1**, all of the $\{\text{Cu}(\text{cyclam})\}$ centrosymmetric complexes present in the structures of **2–4** (Cu1A, Cu1B and Cu1C) also display elongated octahedral CuN_4O_2 coordination geometries with *trans-III* configuration and similar bond lengths in general (Table S1 in the Supplementary Information). Even though the inorganic building block is common to all four compounds, the comparison between the metavanadate chains reveals significant structural differences that are attributable to the intrinsic flexibility of this polymeric anion, which allows it to modify the orientation of the $\{\text{VO}_4\}$ polyhedra as the water molecules of hydration are removed. Thus, although the V–O distances and O–V–O angles do not change significantly when going from **1** to **4** (Table S3–S6 in the Supplementary Information), the torsion angles between consecutive groups of V and O_b atoms along the chains are remarkably modified as shown in Table S7 in the Supplementary Information.

Regarding compound **2**, significant structural changes take place upon partial dehydration compared to the structure of the parent compound **1**. Besides the fact that the number of crystallographically independent metavanadate fragments is reduced to one unique chain with a decrease in the periodicity from 6 to 3 $\{\text{VO}_4\}$ units, the transition from **1** to **2** also involves drastic changes in some of the cell parameters. While the parameter *b* remains almost invariable, *a* and *c* are halved, and thus the volume of the unit cell is reduced almost four times compared to **1** (Table 1). This is reflected in a contraction of the polymeric anions in the crystal packing with a clear shortening of the distance between consecutive equivalent V atoms in the metavanadate chains (Fig S11 in the Supplementary Information). For example, the distance between a given V atom and the nearest equivalent in the chain of **1** with a periodicity of 6 is 16.445 \AA , whereas **2** displays an analogous distance between a V atom and its second nearest equivalent (periodicity 3) of only 16.040 \AA . The significant variations in the torsion $\text{O}_b\text{--V--O}_b\text{--V}$ angles along the chains are at the origin of the observed metavanadate contraction when **1** is transformed into **2** (Table S7 in the Supplementary Information). Due to the crystal rearrangement, the copper atoms in **2** link equivalent chains arranged in antiparallel fashion as opposed to the assembly determined for **1**. Therefore, the crystal packing of **2** shows only one type of hexagonal channel along the *x* axis in which the remaining water molecules of hydration reside (Fig. 5a and Fig. S12 in the Supplementary Information). Nevertheless, the overall hybrid framework of **2** is still highly reminiscent of that described for the parent compound **1** because each channel is delimited by six metavanadate chains linked to each other through the coordination spheres of six alternating $\{\text{Cu}(\text{cyclam})\}$ moieties. The Cu–O distances in **2** are in general slightly shorter than those observed in **1** (Table S1 in the Supplementary Information), and this fact evidences that the chains approach each other as a result of the removal of two water molecules, which has a noticeable effect in the channel volume of **2**. The channels show an approximate cross section of $10.2 \times 13.8 \text{ \AA}^2$ (distances O1...O3 and N1C...N1C) and hence one of the dimensions remarkably shortens compared to those found in either Ch1 or Ch2 in **1**. Moreover, the solvent accessible volume for **2** is 339 \AA^3 , which corresponds to a 22% of the unit cell volume, and this value is somewhat smaller than the 26% found in **1**. This porous structure is still held together by several C–H...O and N–H...O contacts, the geometrical parameters of which are listed in Table S8 in the Supplementary Information.

The SCSC transformation of **2** into **3** upon further dehydration results in additional relevant changes in the overall hybrid framework. The fluxional metavanadate chains stretch back along the [100] direction when going from **2** to **3** (Fig. S11 in the Supplementary Information) and this increases the lattice parameter *a* from 8.02 to 8.60 \AA . Consequently, the distance between consecutive equivalent V atoms in the polymeric anion (17.251 \AA) is lengthened remarkably compared to that observed for **2** (16.040 \AA) and is even much

longer than that found in the parent hybrid **1** (16.445 Å). This lengthening of the V...V distances is accompanied by a general increase of the torsion O_b-V-O_b-V angles (Table S7 in the Supplementary Information). The other cell parameters b and c are slightly reduced when **2** is transformed into **3** (Table 1), which indicates that the hybrid framework undergoes subtle compression in those directions. This compression translates into a slight decrease of the unit cell volume from 1502 to 1365 Å³. The solvent accessible channels are still present in **3** and are still formed through the linkage of six chains by alternating {Cu(cyclam)} complexes in an analogous hexagonal fashion (Fig. 5b and Fig. S13 in the Supplementary Information). However, the stretching of the metavanadate anions displaces the Cu1A atom from being coordinated to the V3 tetrahedron to anchor at the V2 neighbour. Thus, the transformation of **2** into **3** implies the cleavage and formation

of certain Cu–O bonds (Cu1A–O3M and Cu1A–O2M, respectively, see Table S1 in the Supporting Information) which appears to be due to a sliding motion between the metavanadate chains as they stretch. This reallocation of the copper atoms leaves the V3 tetrahedron without any grafted complex while both Cu1C and Cu1A moieties become coordinated to V2. The result of this atom migration is a drastic change in the solvent accessible volume of the channels, which occupy only a 9% of the unit cell volume of **3** (approximately 118 Å³). This is a substantial decrease when compared to the value of 22% found in **2**. Indeed, the approximate dimensions of the channels present in the hybrid framework of **3** decrease to 8.5 x 12.2 Å² (distances O3...O3 and N4C...N4C). The intermolecular C–H...O and N–H...O interactions found in the structure of **3** are listed in Table S9 in the Supplementary Information.

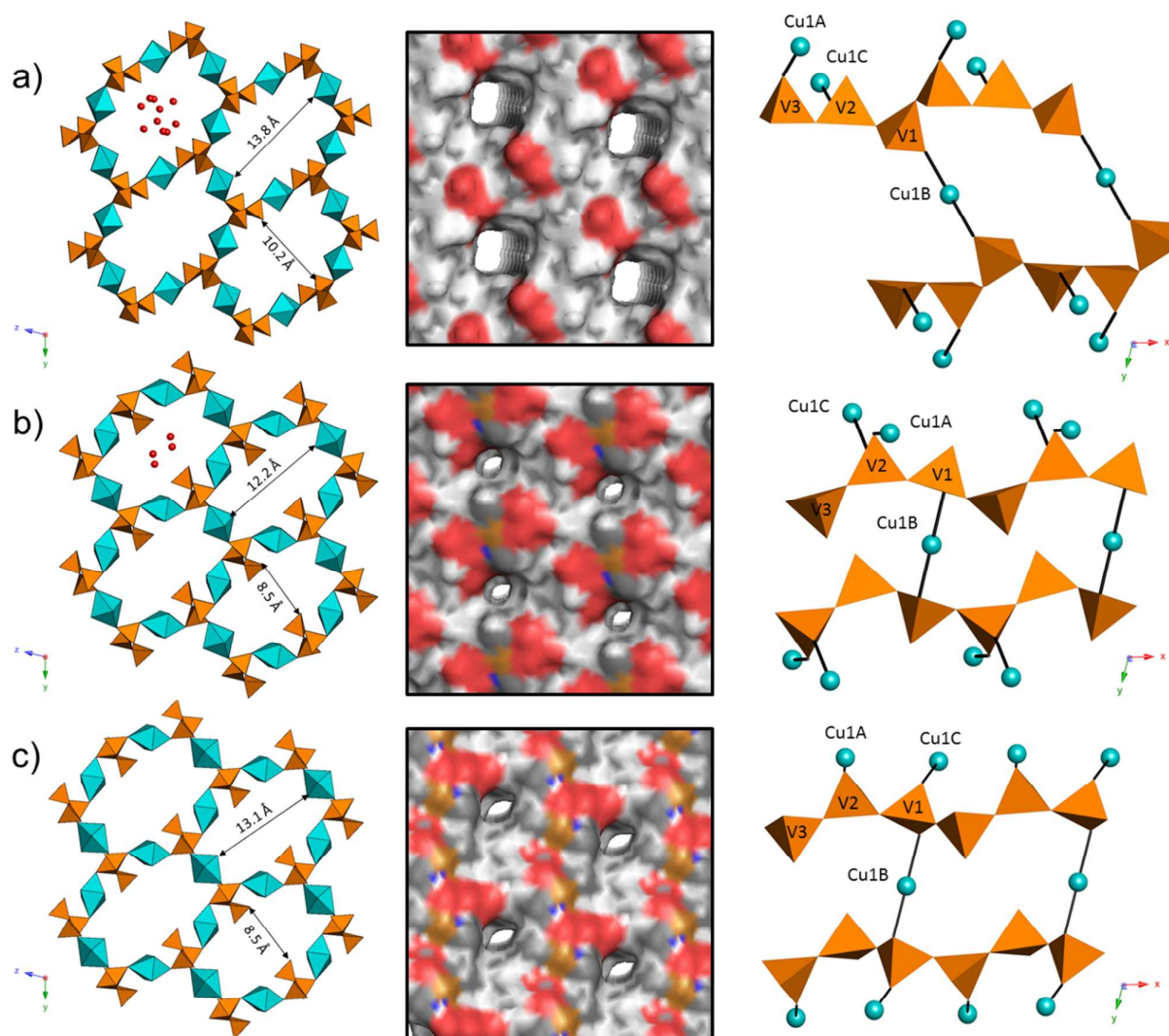


Fig. 5 Left: Crystal packing of compounds **2** (a), **3** (b) and **4** (c) viewed along the x axis with details of the channel dimensions and the hosted water molecules; Centre: Surface of the hybrid frameworks showing the channels; Right: connectivity between the metavanadate chains through different Cu atoms with atom labelling. The cyclam ligands are omitted for clarity in the polyhedral representations. Colour code: $\{VO_4\}$ (orange), Cu (blue).

When **3** is heated to 120 °C, all water molecules are removed from the channels and the anhydrous phase **4** is obtained. In close analogy to the transformation of **2** into **3**, the removal of the remaining water molecules produces the migration of the Cu1C atom from the V2 tetrahedron to the nearest V1 neighbour with consequent cleavage and formation of Cu–O bonds (Cu1C–O2M and Cu1C–O1M, respectively; see Fig. 5c and S14 in the Supplementary Information). In parallel, the Cu1B–O1 bond lengthens significantly to 2.635(11) Å as opposed to the Cu1A–O2M bond, which shortens to 2.493(10) Å. It is worth noting that these structural modifications results in a substantial increase of the solvent accessible volume in the channels from the 9% of the unit cell in **3** to a 15% in **4** (206 Å³ approximately). This enlargement is due to the lengthening of only one of the dimensions of the channels, which are approximately 8.5 x 13.1 Å² in **4** (distances O3···O3 and N4C···N4C). The intermolecular C–H···O and N–H···O interactions found in the anhydrous structure **4** are listed in Table S10 in the Supplementary Information.

Reversibility of the SCSC transformations

Simple TGA/DTA experiments were performed to explore the reversibility of the sequential SCSC transformations observed during the dehydration of **1**. Crystalline samples of this compound were heated at a rate of 2 °C min⁻¹ up to 150 °C, and the so-generated anhydrous samples were kept for a few days in an open container and then heated again at the same rate. The TGA profiles recorded for these anhydrous samples exposed to ambient atmosphere for 1 and 4 days are virtually identical (Fig. S15 in the Supplementary Information) and differ greatly from the mass loss observed in the initial TGA curve. The initial amount of water is 15.72% but only a 5.30% is recovered upon exposure to air. This value is almost identical to the water content in the intermediate phase **3**. Indeed, the TGA curves of freshly prepared samples of **2** and **3** (see Experimental Section) show mass losses of 10.10 and 5.10% that respectively correspond to 3 (calc. 10.46%) and 1.3 (calc. 4.82%) water molecules per two vanadium atoms. These observations are in good agreement with the water molecules determined by single-crystal X-ray diffraction data for both compounds. In view of these results, we concluded that the anhydrous phase is not able to undergo full rehydration or needs longer periods to revert to the original hydrated compound **1** or to the intermediate derivative **2**.

To corroborate the latter hypothesis, we monitored the reversibility of such transformations by combined TGA and PXRD experiments performed once per week during *ca.* one month on samples of compounds **2–4** that were prepared as described in the Experimental Section and stored in an open container exposed to ambient moisture. Among other modifications, the sequential PXRD patterns of **2** evidenced a gradual decrease in the intensity of its characteristic diffraction maximum at 8.0° accompanied by the appearance and gradual increase in intensity of a new diffraction maximum at 7.4° that corresponds to the original compound **1**. After 21 days, the pattern fully corresponded to that expected for the latter

compound and traces of **2** could not be detected any longer (Fig. S16 in Supplementary Information). The sequential TGA profiles are in good agreement with the observations above, as they show a gradual increase of the first stage originating from the loss of the water content. While the TGA curve corresponding to the freshly prepared **2** ($t = 0$) showed a first mass loss of 10.10%, this value was 12.34% for that recorded after 7 days of exposure to air ($t = 7$ days). After two weeks, the amount of water increased to a 13.72% ($t = 14$ days), and after another week, we were able to record a TGA curve virtually identical to that of pure **1** with a water content of 15.86% ($t = 21$ days). All these results confirm that the SCSC transformation of compound **1** into the phase **2** is fully reversible, in such a way that this partially dehydrated derivative slowly converts back into the original hydrated compound in open air conditions.

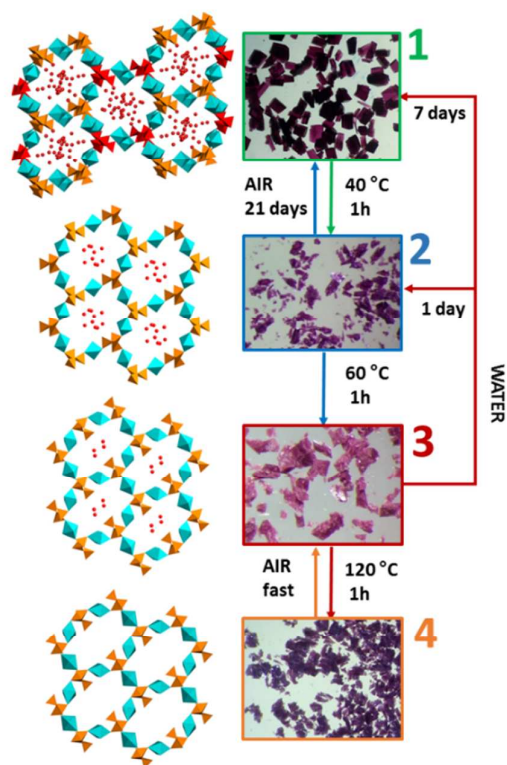


Fig. 6 Scheme of the reversibility of the SCSC transformations between 1–4 with photographs of the crystals for each of the four compound.

Analogous experiments were performed on **3** but no indication of reversibility was found in this case because the PXRD patterns and the TGA curves remained virtually unaltered for at least 37 days. To verify whether the transformation of **1** into **3** was indeed permanent, a sample of the latter phase was soaked in water. The PXRD pattern taken after only 1 day did not show any diffraction maxima corresponding to **3**, but the main signals could only be assigned to a mixture of both **1** and **2**, the latter being the

major component according to the relative intensities of the maxima. After five days, compound **1** becomes the major phase in the mixture, and after seven days ($t = 7$ days), no traces of compound **2** could be detected through PXRD experiments. TGA analyses were also carried out on the polycrystalline sample $t = 7$ days and the results unequivocally confirmed that **3** reverts to the parent **1** upon being immersed in excess of water for a week. The TGA curve of compound **3** shows a mass loss associated with dehydration of 5.10% (1.3 H₂O per 2 V atoms), whereas the sample $t = 7$ days (dried in air) displayed a TGA profile nearly identical to that of compound **1** with a weight loss of 15.68% that corresponds to 5 water molecules per 2 V atoms (Fig. S17 in the Supplementary Information). In the case of **4**, this anhydrous phase rapidly rehydrates to **3** in some hours, as evidenced by the TGA results which are in perfect agreement with those expected for the latter intermediate derivative. All in all, the results of these PXRD and TGA combined experiments demonstrate the reversible nature under the appropriate conditions of the three sequential SCSC transformations that **1** undergoes upon thermal dehydration (Fig 6).

Conclusions

We have successfully prepared and characterized a porous three-dimensional polyoxovanadate hybrid in which gradual loss of water molecules of hydration upon heating triggers a series of sequential single-crystal-to-single-crystal structural transformations. This compound, namely $\{[\text{Cu}(\text{cyclam})](\text{VO}_3)_2\} \cdot 5\text{H}_2\text{O}$ (**1**), undergoes three consecutive and reversible phase transitions that can be followed by single-crystal X-ray diffraction and take place at 40, 60 and 120 °C. These transformations result in the formation of three new porous phases with channels of different sizes, which are $\{[\text{Cu}(\text{cyclam})](\text{VO}_3)_2\} \cdot 3\text{H}_2\text{O}$ (**2**), $\{[\text{Cu}(\text{cyclam})](\text{VO}_3)_2\} \cdot 1.3\text{H}_2\text{O}$ (**3**) and $\{[\text{Cu}(\text{cyclam})](\text{VO}_3)_2\}$ (**4**). While the hybrid open frameworks of **1** and the partially dehydrated **2** are highly reminiscent, the transformation of **2** into **3** involves the migration of Cu^{II} centres, which drastically decreases the size of the channel. Analogously, total dehydration of **3** also promotes the rupture and formation of Cu–O bonds and consequent migration of Cu centres, but in this case the channels enlarge when the anhydrous **4** is formed. In terms of stability, **1** and **3** are stable in ambient conditions, whereas **2** constitutes a metastable state that slowly transforms back into **1** upon exposure to air. The anhydrous phase **4** rapidly adsorbs ambient moisture and reverts to **3** after some hours, whereas the latter can only be converted back into the original compound **1** when immersed in water. The porous nature of **1** and its thermal derivatives, together with the reversibility of their solid-state phase transitions, could render catalytic, sensing or sorption applications for these compounds. In this sense, we intend to investigate in the near future the selective adsorption of certain organic molecules by means of molecular size discrimination.

Acknowledgements

This work was funded by Eusko Jaurilaritza/Gobierno Vasco (Grant IT477-10), MINECO (Grant MAT2013-48366-C2-2-P), and UPV/EHU (UFI11/53). Technical and human support provided by SGIker (UPV/EHU) is gratefully acknowledged.

Notes and references

- (a) J. Vittal, *Coord. Chem. Rev.*, 2007, **251**, 1781–1795; (b) Y. C. Ou, D. S. Zhi, W. T. Liu, Z. P. Ni and M. L. Tong, *Chem. Eur. J.*, 2012, **18**, 7357–7361; (c) M. Du, C. P. Li, J. M. Wu, J. H. Guo and G. C. Wang, *Chem. Commun.*, 2011, **47**, 8088–8090; (d) C. Wang, L. Li, J. G. Bell, X. Lv, S. Tang, X. Zhao and K. M. Thomas, *Chem. Mater.*, 2015, **27**, 1502–1516; (e) J.-P. Zhang, P.-Q. Liao, H.-L. Zhou, R.-B. Lin and X.-M. Chen, *Chem. Soc. Rev.*, 2014, **43**, 5789–5814.
- (a) D. Armentano, G. D. Munno, T. F. Mastropietro, M. Julve and F. Lloret, *J. Am. Chem. Soc.*, 2005, **127**, 10778–10779; (b) X. N. Cheng, W. X. Zhang, Y. Y. Lin, Y. Z. Zheng and X. M. Chen, *Adv. Mater.*, 2007, **19**, 1494–1498; (c) G. C. Lv, P. Wang, Q. Liu, J. Fan, K. Chen and W. Y. Sun, *Chem. Commun.*, 2012, **48**, 10249–10251; (d) Y. Q. Lan, H. L. Jiang, S. L. Li and Q. Xu, *Inorg. Chem.*, 2012, **51**, 7484–7491; (e) M. H. Xie, X. L. Yang and C. D. Wu, *Chem. Eur. J.*, 2011, **17**, 11424–11427; (f) L. X. Shi, W. F. Zhao, X. Xu, J. Tang and C. D. Wu, *Inorg. Chem.*, 2011, **50**, 12387–12389; (g) A. Aslani and A. Morsali, *Chem. Commun.*, 2008, 3402–3404.
- (a) Y. J. Zhang, T. Liu, S. Kanegawa and O. Sato, *J. Am. Chem. Soc.*, 2009, **131**, 7942–7943; (b) M. Wriedt, A. A. Yakovenko, G. J. Halder, A. V. Prosvirin, K. R. Dunbar and H. C. Zhou, *J. Am. Chem. Soc.*, 2013, **135**, 4040–4050.
- (a) S. M. Neville, G. J. Halder, K. W. Chapman, M. B. Duriska, P. D. Southon, J. D. Cashion, J. F. Letard, B. Moubaraki, K. S. Murray and C. J. Kepert, *J. Am. Chem. Soc.*, 2008, **130**, 2869–2876; (b) J. Campo, L. R. Falvello, I. Mayoral, F. Palacio, T. Soler and M. Tomas, *J. Am. Chem. Soc.*, 2008, **130**, 2932–2933; (c) D. Sarma and S. Natarajan, *Cryst. Growth Des.*, 2011, **11**, 5415–5423; (d) K. D. Demadis, M. Papadaki, M. A. Aranda, A. Cabeza, P. Olivera-Pastor and Y. Sanakis, *Cryst. Growth Des.*, 2010, **10**, 357–364.
- (a) A. S. J. Wéry, J. M. Gutiérrez-Zorrilla, A. Luque, M. Ugalde and P. Román, *Chem. Mater.*, 1996, **8**, 408–413; (b) C. Ritchie, C. Streb, J. Thiel, S. G. Mitchell, H. N. Miras, D.-L. Long, T. Boyd, R. D. Peacock, T. McGlone and L. Cronin, *Angew. Chem. Int. Ed.*, 2008, **47**, 36, 6881–6884; (c) L.-Z. Zhang, W. Gu, X. Liu, Z. Dong and B. Li, *CrystEngComm*, 2008, **10**, 652–654; (d) J. Thiel, C. Ritchie, C. Streb, D.-L. Long and L. Cronin, *J. Am. Chem. Soc.*, 2009, **131**, 4180–4181; (e) K. Uehara and N. Mizuno, *J. Am. Chem. Soc.*, 2011, **133**, 1622–1625.
- (a) L.-Z. Zhang, W. Gu, Z. Dong, X. Liu and B. Li, *CrystEngComm*, 2008, **10**, 1318–1320; (b) S. Reinoso, M. H. Dickman, A. Praetorius and U. Kortz, *Acta Crystallogr.*, 2008, **E64**, m614. (c) D. Barats-Damatov, L. J. Shimon, Y. Feldman, T. Bendikov and R. Neumann, *Inorg. Chem.*, 2015, **54**, 628–634; (d) C.-L. Chen, A. M. Goforth, M. D. Smith, C.-Y. Su and H.-C. zur Loye, *Angew. Chem. Int. Ed.*, 2005, **44**, 6673–6677.
- (a) M. T. Pope, *Heteropoly and Isopoly Oxometalates*, Springer-Verlag, Berlin, Germany, 1983; (b) *Polyoxometalates: From Platonic Solids to Anti-Retroviral Activity*, ed. M. T. Pope and A. Müller, Kluwer, Dordrecht, The Netherlands, 1994; (c) *Polyoxometalate Chemistry: from Topology via Self-Assembly to Applications*, ed. M. T. Pope and A. Müller, Kluwer, Dordrecht, The Netherlands, 2001; (d) *Polyoxometalate Chemistry for Nanocomposite Design*, ed. M. T. Pope and T. Yamase, Kluwer, Dordrecht, The Netherlands, 2002; (e) *Polyoxometalate Molecular Science*, ed. J. J. Borrás-Almenar, E. Coronado, A. Müller and M. T. Pope, Kluwer, Dordrecht, The Netherlands, 2003; (f) Guest ed. U. Kortz, *Eur. J. Inorg. Chem.*, 2009, thematic issue 5; (g) Guest ed. L. Cronin and D.-L. Long, *Dalton Trans.*, 2012, **41**, thematic issue 33; (h) Guest ed. L. Cronin and A. Muller, *Chem. Soc. Rev.*, 2012, **41**, thematic issue 24.

- 8 (a) J. M. Clemente-Juan and E. Coronado, *Coord. Chem. Rev.*, 1999, **193**–195, 361–394; (b) U. Kortz, A. Müller, J. Van Slageren, J. Schnacke, N. S. Dalal and M. Dressel, *Coord. Chem. Rev.*, 2009, **253**, 2315–2327; (c) P. Mialane, A. Dolbecq and F. Sécheresse, *Chem. Commun.*, 2006, 3477–3485; (d) P. Kögerler, B. Tsukerblat and A. Müller, *Dalton Trans.*, 2010, **39**, 21–36; (e) C. L. Hill, *J. Mol. Catal. A*, 2007, **262**, 2–6; (f) E. Coronado and C. J. Gómez-García, *Chem. Rev.*, 1998, **98**, 273–296; (g) A. Müller and F. Peters, *Chem. Rev.*, 1998, **98**, 239–271; (h) M. Inoue, T. Suzuki, Y. Fujita, M. Oda, N. Matsumoto and T. Yamase, *J. Inorg. Biochem.*, 2006, **100**, 1225–1233.
- 9 (a) H. N. Miras, L. Vilá-Nadal and L. Cronin, *Chem. Soc. Rev.*, 2014, **43**, 5679–5699; (b) M. I. Khan, L. M. Meyer, R. C. Haushalter, A. L. Schweitzer, J. Zubieta and J. L. Dye, *Chem. Mater.*, 1996, **8**, 43–53; (c) B.-X. Dong, L. Chen, S. Y. Zhang, J. Ge, L. Song, H. Tian, Y.-L. Teng and W.-L. Liu, *Dalton Trans.*, 2015, **44**, 1435–1440; (d) D.-Y. Du, J.-S. Qin, S.-L. Li, Z.-M. Su and Y.-Q. Lan, *Chem. Soc. Rev.*, 2014, **43**, 4615–4632; (e) G.-C. Ou, L. Jiang, X.-L. Feng and T.-B. Lu, *Dalton Trans.*, 2009, 71–76; (f) J. Li, X. Huang, S. Yang, Y. Xu and C. Hu, *Cryst. Growth Des.*, 2015, **15**, 1907–1914.
- 10 (a) B. Nohra, H. El Moll, L. M. Rodriguez, P. Mialane, J. Marrot, C. Mellot-Draznieks, M. O’Keeffe, R. N. Biboum, J. Lemaire, B. Keita, L. Nadjó and A. Dolbecq, *J. Am. Chem. Soc.*, 2011, **133**, 13363–13374; (b) S. Cardona-Serra, J. M. Clemente-Juan, E. Coronado, A. Gaita-Ariño, N. Suaud, O. Svoboda, R. Bastardis, N. Guihéry and J. J. Palacios, *Chem. Eur. J.*, 2015, **21**, 763–769; (c) D. M. Fernandes, A. D. Barbosa, J. Pires, S. S. Balula, L. Cunha-Silva and C. Freire, *Appl. Mater. Interfaces*, 2013, **5**, 13382–13390; (d) M. I. Khan, N. R. Putrevu, S. Ayesh, E. H. Yohannes, R. Cage and R. Doedens, *Cryst. Growth Des.*, 2013, **13**, 4667–4672.
- 11 (a) A. Iturraspe, B. Artetxe, S. Reinoso, L. San Felices, P. Vitoria, L. Lezama and J. M. Gutiérrez-Zorrilla, *Inorg. Chem.*, 2013, **52**, 3084–3093; (b) A. Iturraspe, L. San Felices, S. Reinoso, B. Artetxe, L. Lezama and J. M. Gutiérrez-Zorrilla, *Cryst. Growth Des.*, 2014, **14**, 2318–2328.
- 12 (a) M. T. Pope and A. Müller, *Angew. Chem. Int. Ed. Engl.*, 1991, **30**, 34–48; (b) S. X. Liu, L. H. Xie, B. Gao, C. D. Zhang, C. Y. Sun, D. H. Li and Z. M. Su, *Chem. Commun.*, 2005, 5023–5025; (c) W. G. Klemperer, T. A. Marquart and O. M. Yaghi, *Angew. Chem. Int. Ed. Engl.*, 1992, **31**, 49–51; (d) L. Chen, F. L. Jiang, Z. Z. Lin, Y. F. Zhou, C. Y. Yue and M. C. Hong, *J. Am. Chem. Soc.*, 2005, **127**, 8588–8589; (f) P. Wu, Z. Xiao, J. Zhang, J. Hao, J. Chen, P. Yin and Y. Wei, *Chem. Commun.*, 2011, **47**, 5557–5559; (g) U. Lee, H. C. Joo, K. M. Park, S. S. Mal, U. Kortz, B. Keita and L. Nadjó, *Angew. Chem. Int. Ed.*, 2008, **47**, 793–796. (h) L. Zhang and W. Schmitt, *J. Am. Chem. Soc.*, 2011, **133**, 11240–11248. (i) S. Konar and A. Clearfield, *Inorg. Chem.*, **47**, 2008, 3492–3494; (j) A. Müller, K. Hovemeier and R. Rohlffing, *Angew. Chem. Int. Ed. Engl.*, 1992, **31**, 1192–1195.
- 13 (a) J. J. Christensen, D. J. Eatough and R. M. Izatt, *Chem. Rev.*, 1974, **74**, 351–384; (b) D. K. Cabbiness and D. W. Margerum, *J. Am. Chem. Soc.*, 1969, **91**, 6540–6541; (c) J. D. Silversides, C. C. Allan and S. J. Archibald, *Dalton Trans.*, 2007, 971–978.
- 14 (a) E. Kimura, C. A. Dalimunte, A. Yamashita and R. Machida, *J. Chem. Soc., Chem. Commun.*, 1985, 1041–1043; (b) E. Kimura, M. Sasada, M. Shionoya, T. Koike, H. Kurosaki and M. Shiro, *J. Biol. Inorg. Chem.*, 1997, **2**, 74–82; (c) E. Kimura, M. Shionoya, T. Mita and Y. Iitaka, *J. Chem. Soc., Chem. Commun.*, 1987, 171–172.
- 15 (a) C. Bolm, N. Meyer, G. Raabe, T. Weyhermüller and E. Bothe, *Chem. Commun.*, 2000, 2435–2436; (b) A. Grenz, S. Ceccarelli and C. Bolm, *Chem. Commun.*, 2001, 1726–1727; (c) R. Breslow, D. Berger and D. L. Huang, *J. Am. Chem. Soc.*, 1990, **112**, 3686–3687; (d) K. Mochizuki, S. Manaka, I. Takeda and T. Kondo, *Inorg. Chem.*, 1996, **35**, 5132–5136.
- 16 (a) W. A. Volkert and T. J. Hoffmann, *Chem. Rev.*, 1999, **99**, 2269–92; (b) Y. Inouye, T. Kanamori, T. Yoshida, X. Bu, M. Shionoya, T. Koike and E. Kimura, *Biol. Pharm. Bull.*, 1994, **17**, 243–250.
- 17 *CrysAlisPro Software System*, Agilent Technologies UK Ltd., Oxford, U. K., 2012.
- 18 O. V. Dolomanov, L. J. Bourhis, R. J. Gildea, J. A. Howard, H. J. Puschmann, *J. Appl. Crystallogr.*, 2009, **42**, 339–342.
- 19 G. M. Sheldrick, *Acta Crystallogr.*, 2008, **A64**, 112–122.
- 20 C. F. Macrae, I. J. Bruno, J. A. Chisholm, P. R. Edgington, P. McCabe, E. Pidcock, L. Rodriguez-Monge, R. Taylor, J. Van de Streek and P. A. Wood, *J. Appl. Crystallogr.*, 2008, **41**, 466.
- 21 A. L. Spek, *Acta Crystallogr.*, 2009, **D65**, 148–155.
- 22 L. J. Farrugia, *J. Appl. Crystallogr.*, 1999, **32**, 837–838.
- 23 K. H. Bosco and F. Gruswitz, *BMC Struct. Biol.*, 2008, **8**, 49.
- 24 *The PyMOL Molecular Graphics System*, Version 1.7.1, Schrödinger, LLC, 2014.
- 25 J. A. A. Ketelaar, *Chem. Weekbl.*, 1936, **33**, 51–57.
- 26 D. Mercurio-Lavaud and B. Frit, *CR Seances Acad. Sci., Ser. C*, 1973, **277**, 1101.
- 27 C. Brisi and A. Molinari, *Ann. Chim. Rome*, 1958, **48**, 263–269.
- 28 B. Bosnich, C. K. Poon and M. L. Tobe, *Inorg. Chem.*, 1965, **4**, 1102–1108.
- 29 M. Bakaj and M. J. Zimmer, *J. Mol. Struct.*, 1999, **508**, 59–72.

Graphical Abstract

The polyoxovanadate hybrid $[\{\text{Cu}(\text{cyclam})\}(\text{VO}_3)_2] \cdot 5\text{H}_2\text{O}$ (**1**) with porous three-dimensional framework undergoes a series of sequential and reversible single-crystal-to-single-crystal transformations upon thermally triggered gradual dehydration. These transitions can be followed by single-crystal X-ray diffraction and take place at 27 (**2**), 49 (**3**) and 73 °C (**4**) to result in three new phases with channels of different sizes.

